Vibrational predissociation in argon complexes of 3aminostetrazine and 3amino6 methylstetrazine: Evidence for extreme modeselectivity

Joseph C. Alfano, Selso J. Martinez III, and Donald H. Levy

Citation: The Journal of Chemical Physics **96**, 2522 (1992); doi: 10.1063/1.462004
View online: http://dx.doi.org/10.1063/1.462004
View Table of Contents: http://scitation.aip.org/content/aip/journal/jcp/96/4?ver=pdfcov
Published by the AIP Publishing

Vibrational predissociation in argon complexes of 3-amino-*s*-tetrazine and 3-amino-6-methyl-*s*-tetrazine: Evidence for extreme mode-selectivity

Joseph C. Alfano, Selso J. Martinez III, and Donald H. Levy
The James Franck Institute and the Department of Chemistry, The University of Chicago, Chicago, Illinois 60637

(Received 23 July 1991; accepted 26 September 1991)

We have investigated the vibrational predissociation of argon complexes of 3-amino-*s*-tetrazine (AT) and 3-amino-6-methyl-*s*-tetrazine (AMT). Twelve vibrational levels of complexes of the form AT–Ar_n, where $n = 1$, 2, and 3, were examined. The dissociation rate of the binary AT–Ar complex varied from $3\times10^6\ s^{-1}$ to $>4\times10^8\ s^{-1}$ depending on the initially excited mode, with the fastest rate corresponding to the lowest energy vibration. Even levels with vibrational energies over five times that needed to break the van der Waals bond still showed significant amounts of fluorescence from the unfragmented complex. Photodissociation of the AT–Ar_2 complex can yield two different dissociation products, AT and AT–Ar. The ratio of these photoproducts varied greatly among different vibrational modes. The $16b^2$ level of AT–Ar_2 at $+462\ cm^{-1}$ gives primarily the AT photoproduct, while the $16a^2$ level at $+505\ cm^{-1}$ gives exclusively the AT–Ar photoproduct. The two levels of AT–Ar_3 which were studied both appear to show only partial fragmentation. We examined the basic spectroscopy of AMT using vibrationally resolved fluorescence excitation spectroscopy, and assigned a number of vibrational levels in both the ground and excited states. We then used this information to measure the branching ratios and dissociation rates for seven vibrational levels of AMT–Ar. These vibrational predissociation rates show strong qualitative differences from similar data for tetrazine–Ar and aminotetrazine–Ar complexes. Finally, these results were compared to similar work on other tetrazine derivatives to attempt to account for this strong mode-selective behavior.

I. INTRODUCTION

In the search for vibrational mode-selective chemical behavior, spectroscopists have focused attention on weakly bound van der Waals complexes. The photodissociation of van der Waals complexes holds promise for mode selectivity, as vibrational predissociation can occur at very low energies in a region of the potential where anharmonic mixings among the intramolecular modes are small. Thus it is possible to excite zeroth order intramolecular modes which do not undergo immediate vibrational randomization.

However, conclusive observations of dramatic mode selective behavior in van der Waals complexes have been elusive. The most widely studied class of complexes has been single ring aromatic molecules complexed with a single rare gas atom. The first system of this type studied was *s*-tetrazine–argon[1–5] (*s*-tetrazine is shown in Fig. 1). Here, the vibrational predissociation rate for the five vibrational levels studied varied by about a factor of 2; little mode selectivity was observed. The results[6] for benzene–Ar mirror those of tetrazine–Ar. Excitation of several levels near $+1440\ cm^{-1}$ give very similar dissociation rates of $\sim10^8\ s^{-1}$, indicating little dependence on the initially excited mode. Pyridine–Ar,[7] p-difluorobenzene–Ar,[8–10] and aniline–Ar[11] give similar results, with the mode selectivity of the dissociation rate being measurable but not dramatic. With one exception these rates vary by less than a factor of 5 as a function of the initially excited level, all being $\sim10^8\ s^{-1}$.

Recently we undertook an investigation of the dissociation dynamics of complexes of 3-amino-*s*-tetrazine[12] (AT) with argon. AT, which is shown in Fig. 1, has a fluorescence quantum yield that is much higher than that of tetrazine.[13] Because of the high signal levels, we were able to examine not only the binary complex AT–Ar, but also higher argon clusters including AT–Ar_2 and AT–Ar_3. To our surprise, we found strong mode selective behavior. The vibrational predissociation rate of the AT–Ar complex varies by over two orders of magnitude, depending on the initially excited mode. In the AT–Ar_2 complexes, the ratio between the two possible photoproducts, AT–Ar and AT, shows great mode selectivity. Descriptions of these data have appeared.[14,15]

In an effort to elucidate the factors responsible for the large differences in the dissociation dynamics of tetrazine–argon and AT–Ar, we have undertaken a systematic study of the excited state vibrational predissociation dynamics of complexes between various tetrazine derivatives and rare gas atoms. Recently, we have investigated vibrational predissociation in complexes of dimethyl-*s*-tetrazine and argon.[16] In this article, we give a full report of our work on the AT complexes, and additionally present the results of our studies on complexes between argon and 3-amino-6-methyl-*s*-tetrazine (AMT), shown in Fig. 1. A complete description of the AT–Ar_n ($n = 1,2,3$) dissociation is presented first. We then describe the basic spectroscopy of the AMT monomer, where we use low resolution excitation and emission spectra to assign vibrational levels in the AMT ground and

 0021-9606/92/042522-18$06.00

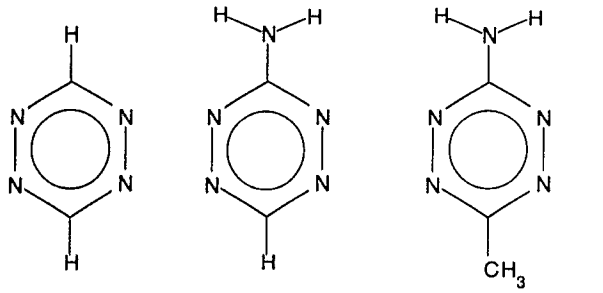

FIG. 1. The tetrazine, AT, and AMT molecules.

excited states. Next, we describe the dissociation of the AMT–Ar complex. Finally, we discuss the results of our analysis in terms of the previous work on vibrational predissociation of van der Waals complexes of other tetrazine derivatives and rare gas atoms.

II. EXPERIMENT

Our experimental apparatus has been described previously,[17-19] and only a brief description will be given here. A supersonic jet seeded with AT or AMT was generated by passing helium over a reservoir of the respective molecule heated to 80 °C and expanding the resulting mixture through a 100 μ pinhole. To generate argon complexes, a few percent of argon gas was bled into the mixture. The resulting supersonic expansion was crossed with the output of an argon-ion pumped cw dye laser operating on either Rhodamine 110 or Coumarin 535. For fluorescence excitation scans, the laser-induced fluorescence was imaged with a camera lens onto a slit, which served to limit laser scattering. The fluorescence passing through the slit was detected by a cooled photomultiplier tube (RCA C31000A) in a photon counting configuration. The fluorescence intensity as a function of laser frequency was normalized for fluctuations in laser power and was digitally recorded. For dispersed emission spectra, an etalon was inserted into the laser cavity to reduce the laser bandwidth to $\sim 0.1\ \mathrm{cm}^{-1}$, and the laser then tuned to the top of the rotational contour of the vibrational feature of interest. The resulting fluorescence was collected and imaged onto the entrance slits of a 1 m monochromator. The dispersed emission spectra were normalized using the simultaneously collected total fluorescence signal. All spectra were digitally recorded on a Dell System 310 personal computer. The samples of AT and AMT were prepared by Dr. D. D. Yang as described in the literature.[20,21]

III. RESULTS

A. AT–Ar cluster dynamics

1. AT–Ar

We have studied the dissociation of five vibrationally excited levels of AT–Ar, ranging from $+446$ to $+1212$ cm^{-1} excess vibrational energy. Some of the normal modes of AT are shown in Fig. 2, and are labeled using Wilson notation. The three lowest-lying levels, $\overline{16b^2}$, $\overline{16a^2}$, and $\overline{6a^1}$, have been described in our previous communications,[14,15] and are summarized here. (Throughout this paper, a bar over a transition refers to that transition in the AT–Ar or AMT–Ar complex; a double bar indicates that transition in the di-argon complex, and so forth.) The dis-

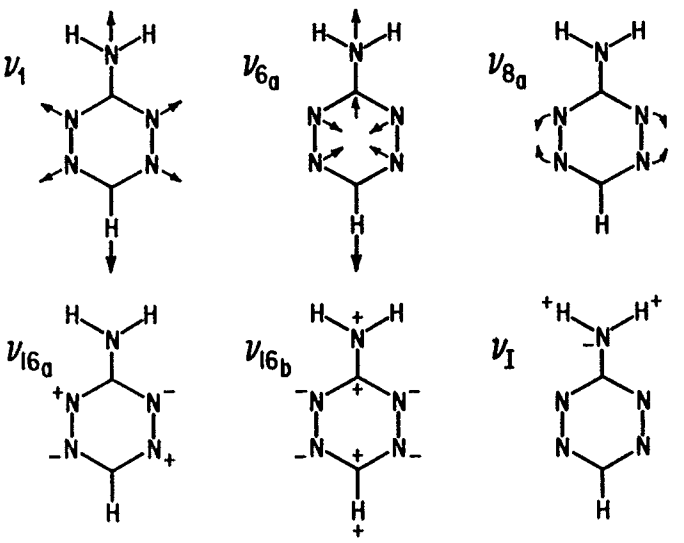

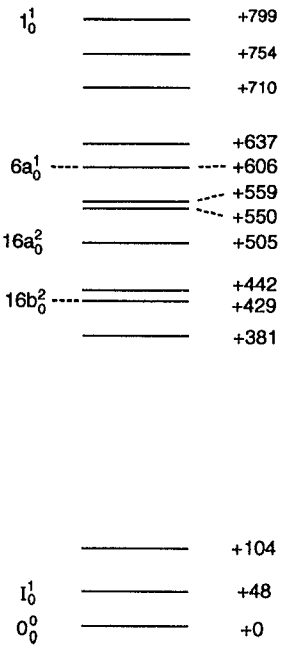

FIG. 2. Some normal modes of the AT molecule, along with an energy level diagram of the low energy vibrations seen in the AT excitation spectrum.

persed emission spectrum of $\overline{16b^2}$ at $+446\ cm^{-1}$ shows transitions which match almost exactly in position and intensity with features seen in the single vibronic level (SVL) emission spectrum of the AT zero-point level.[14] Therefore complex dissociation is much faster than resonance fluorescence, since no features due to the initially excited $\overline{16b^2}$ level are seen. (In all of this analysis we assume that argon complexation does not change the fluorescence lifetimes of the AMT or AT vibrational levels.) Moving up to the $\overline{16a^2}$ level at $+505\ cm^{-1}$, dissociation was found to be less efficient, since the $\overline{16a^2}$ emission spectrum shows small features originating from the initially excited level, in addition to transitions from the AT zero-point level. Finally, the $\overline{6a^1}$ level at $+606\ cm^{-1}$ was found to dissociate much less efficiently than the two lower levels. The emission spectrum of $\overline{6a^1}$ is dominated by resonance fluorescence, with only a small amount of emission from the AT photofragment.

Next we examined the $\overline{1^1}$ level, at $+798\ cm^{-1}$. The emission spectrum of $\overline{1^1}$, seen in Fig. 3(a), shows emission from the 0^0, $16b^1$, and $16a^2$ levels of the AT photodissociation product. Additionally, very weak features can be seen which originate from the initially excited $\overline{1^1}$ level. Our observation of $16a^2$ emission ($505\ cm^{-1}$) following $\overline{1^1}$ excitation ($798\ cm^{-1}$) implies that the excited state van der Waals binding energy, D_0', is $<293\ cm^{-1}$.

Finally, we studied the $\overline{6a^2}$ level at $+1212\ cm^{-1}$. Excitation of $\overline{6a^2}$ produces the complicated emission spectrum shown in Fig. 3. Many of the bands can be assigned as dissociation products, leaving the AT photofragment in the 0^0, $+381$, and $6a^1$ levels. Additionally, a substantial amount of resonance emission can be identified in the feature at the excitation wave number ($<30\%$ of which is scattered laser light), as well as the features at 19 346, 18 923, and 18 732 cm^{-1}. Thus, even at an energy level many times that needed for dissociation, vibrational predissociation is still sufficiently slow compared to the 62 ns lifetime[13] of the $6a^2$ level that resonance fluorescence is observable. There is a significant number of intense peaks which we cannot assign, since only a small number of the frequencies of the vibrational normal modes of AT are known.[12] We believe most of these peaks result from a dissociation product in which the AT photofragment is left in a vibrational mode or modes which are not optically accessible from the ground vibronic state due to poor Franck–Condon factors, and thus have not been previously assigned. The dissociation features in Fig. 3(b) are in general somewhat broader than the instrumental resolution, indicating significant rotational excitation of the AT photofragment.

2. AT–Ar_2

The photodissociation of AT–Ar_2 is more complicated than that of the binary AT–Ar complex, since now two dissociation products (AT and AT–Ar) are possible. Once again, the three lowest-lying levels, $\overline{\overline{16b^2}}$, $\overline{\overline{16a^2}}$, and $\overline{\overline{6a^1}}$, have been previously described.[14,15] The $\overline{\overline{16b^2}}$ emission spectrum shows primarily emission from the vibrationless level of AT, indicating that both van der Waals bonds have been ruptured, with a smaller amount of emission from the vibrationless level of AT–Ar also visible. No emission from the initially excited $\overline{\overline{16b^2}}$ level can be seen. The $\overline{\overline{16a^2}}$ level at $+505\ cm^{-1}$ shows a very clean spectrum

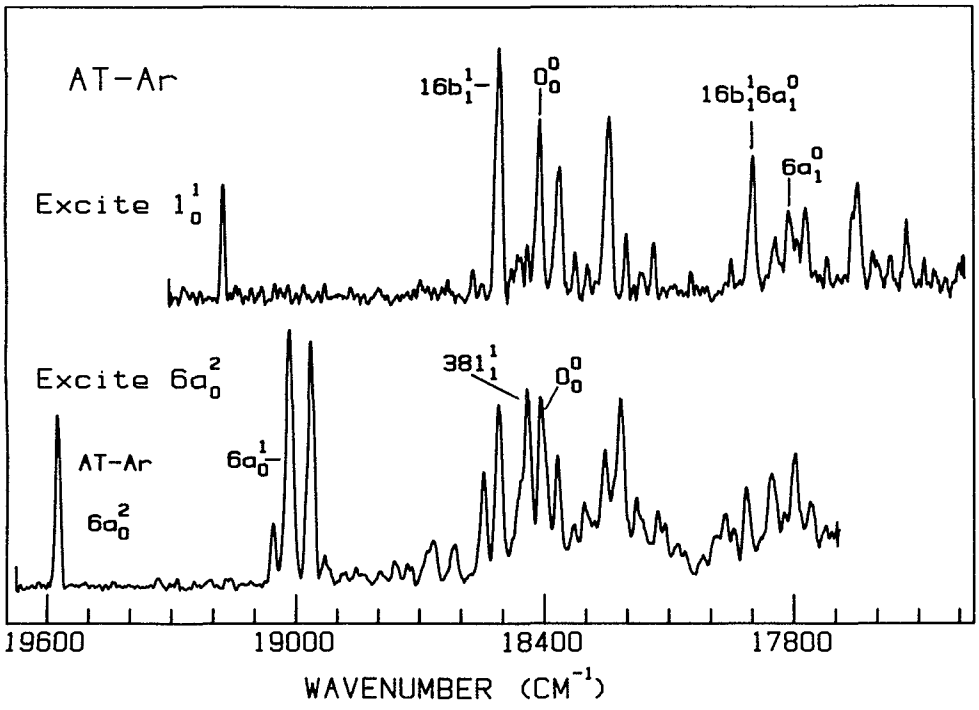

FIG. 3. (a) The emission spectrum obtained by excitation of the 1_0^1 band of AT–Ar, taken at a resolution of 11 cm^{-1}. $<80\%$ of the intensity at the excitation wave number is due to scattered laser light. (b) The emission spectrum obtained by excitation of the $6a_0^2$ band of AT–Ar, taken at a resolution of 15 cm^{-1}. $<30\%$ of the intensity at the excitation wave number is due to scattered laser light.

composed exclusively of emission from the vibrationless level of AT–Ar. Finally, the $\overline{\overline{6a^1}}$ level at $+606\ cm^{-1}$ consists primarily of emission from the AT–Ar zero-point level. A much smaller amount of resonance fluorescence from the initially excited $\overline{\overline{6a^1}}$ level is also seen. Additionally, a very small, somewhat broadened feature centered at $\sim 18\,357\ cm^{-1}$ appears to be vibrationally relaxed $AT–Ar_2$ emission.

We have extended these studies and investigated the $\overline{\overline{1^1}}$ level at $+798\ cm^{-1}$. The emission spectrum of $\overline{\overline{1^1}}$, seen in Fig. 4(a), is composed of transitions which cannot be assigned using the known vibrational frequencies of AT. These features consist primarily of a series of broadened transitions whose intensity and relative wave numbers match those of the vibrationless AT or AT–Ar level. This entire series, however, is shifted 9 cm^{-1} to the red of the AT origin transition, and 18 cm^{-1} to the blue of the AT–Ar origin transition. It is likely that this involves a sequence band of some unknown vibrational level.

Finally, we studied the $\overline{\overline{6a^2}}$ level at $+1212\ cm^{-1}$. Excitation of $\overline{\overline{6a^2}}$ results primarily in fragmentation of both van der Waals bonds, as can be seen in the emission spectrum in Fig. 4(b). Most of the intense features originate from the 0^0, $16b^1$, or $16a^2$ level of bare AT, indicating dissociation of both argon atoms. A very small amount of emission from $\overline{6a^1}$ is seen, where only a single van der Waals bond is ruptured. Finally, a small amount of emission from the initially excited $\overline{\overline{6a^2}}$ levels is seen, indicating that dissociation is not complete during the 59 ns lifetime of the $\overline{\overline{6a^2}}$ level.

3. $AT–Ar_3$

The emission spectrum of the $6a^1$ level of $AT–Ar_3$, at $+606\ cm^{-1}$, is shown in Fig. 5. This spectrum shows an origin-like series of vibrational features. These features, however, are shifted 12 cm^{-1} to the red of the corresponding AT–Ar zero-point transition and 16 cm^{-1} to the blue of the $AT–Ar_2$ zero-point level. These transitions, which are significantly broader than the instrumental resolution, cannot be assigned in terms of known vibrational frequencies of AT, and most likely involve $\Delta v = 0$ sequence bands of an unknown vibrational frequency.

Finally, we have obtained the emission spectrum obtained subsequent to excitation of the $6a^2$ level of $AT–Ar_3$ at $+1212\ cm^{-1}$. This spectrum is identical to the emission spectrum obtained by exciting the $\overline{\overline{1^1}}$ level of $AT–Ar_2$. As mentioned for the $\overline{\overline{1^1}}$ level, the assignments of these transitions are uncertain, and must involve unassigned modes of AT.

B. AMT basic spectroscopy

1. Fluorescence excitation spectrum and excited state assignments

Figure 6 shows the low resolution fluorescence excitation spectrum of AMT, taken at a resolution of $\sim 1\ cm^{-1}$. A listing of the frequencies of the transitions with respect to the origin, their intensities, and our partial assignments is given in Table I of PAPS.[22] To our knowledge, there has been no

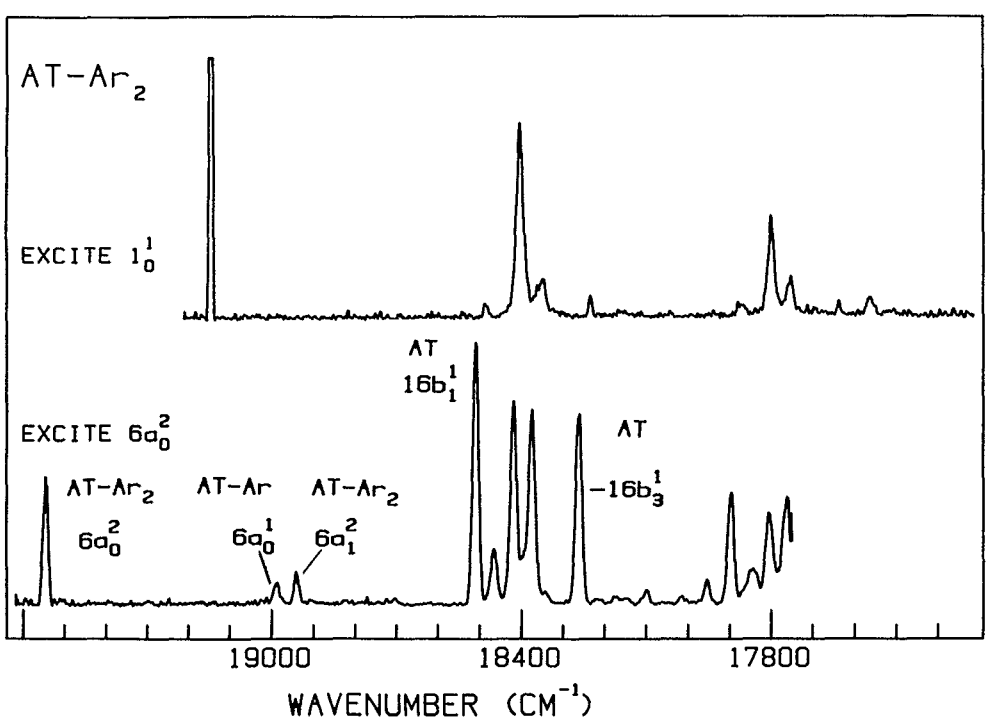

FIG. 4. (a) The emission spectrum obtained by excitation of the 1^1_0 band of $AT–Ar_2$, taken at a resolution of 10 cm^{-1}. All of the intensity at the excitation wave number is due to scattered laser light. (b) The emission spectrum obtained by excitation of the $6a^2_0$ band of $AT–Ar_2$, taken at a resolution of 16 cm^{-1}. At least 85% of the intensity at the excitation wave number is due to scattered laser light.

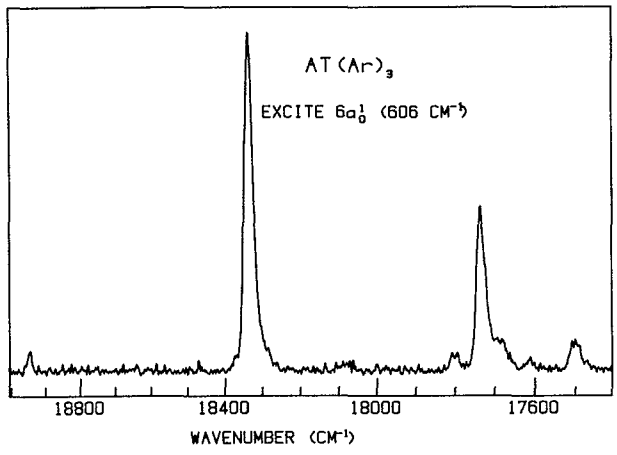

FIG. 5. The emission spectrum obtained by excitation of the $6a_0^1$ band of AT–Ar_3, taken at a resolution of 18 cm^{-1}. All of the intensity at the excitation wave number is due to scattered laser light.

previous gas phase spectroscopic work done on AMT. Hence, we have based our assignments on known vibrational assignments previously given for tetrazine,[17,23,24] 3-methyl-*s*-tetrazine[25] (MT), 3,6-dimethyl-*s*-tetrazine[26] (DMT), AT,[12] and *p*-toluidine.[27]

The intense feature at 18 026 cm^{-1} is assigned as the origin transition of the first excited singlet state. This transition is red-shifted ~400 cm^{-1} from the corresponding origin transition of AT at 18 410 cm^{-1}. The remainder of the features at higher energies are transitions which are vibrationally excited in one or more normal modes. A complete assignment of these transitions is very difficult. However, the extensive work done on tetrazine and its derivatives enable us to make a partial assignment of the features in the fluorescence excitation spectrum. Throughout this discussion, we make use of Wilson notation. Some normal modes are shown in Fig. 2.

a. ν_{6a}. The fluorescence excitation spectrum is dominated by a 531 cm^{-1} progression. All previous tetrazine derivatives exhibit similar prominent progressions in the totally symmetric ν_{6a} vibrational mode, hence we assign this 531 cm^{-1} as belonging to ν_{6a}. The wave number of this mode is similar to that of ν'_{6a} in DMT (519 cm^{-1}) and less than those of ν'_{6a} in tetrazine, MT, and AT (702, 606, and 580 cm^{-1}, respectively). Substitution onto a ring carbon atom will tend to increase the reduced mass of this mode, causing a decrease in frequency. Thus, the values of ν'_{6a} in substituted tetrazine would be expected to have the relationship ν'_{6a}(tetrazine) $>\nu'_{6a}$(MT) $\approx\nu'_{6a}$(AT) $>\nu'_{6a}$(DMT) $\approx\nu'_{6a}$(AMT), as is observed.

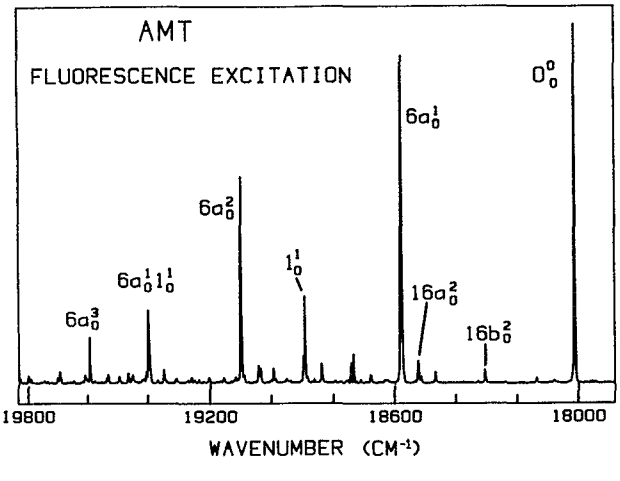

FIG. 6. The low-resolution fluorescence excitation spectrum of AMT, taken at a resolution of ~1 cm^{-1}.

b. ν_1. The largest vibrational feature which is not a member of the $6a_0^n$ progression is at +850 cm^{-1}, and is assigned as the 1_0^1 transition. The wave number of ν'_1 is less than that of tetrazine (1006 cm^{-1}), and similar to that of AT and DMT (799 and 834 cm^{-1}, respectively).

c. ν_{16a}. The nontotally symmetric ν_{16a} mode has a node at the ring carbon atoms, implying that ν'_{16a} should be relatively insensitive to substitution onto the ring carbon atoms. In tetrazine, AT, and DMT, the lowest allowed even overtone $16a_0^2$ occurs at +510, +505, and +495 cm^{-1}, respectively. The closest peak in this region with significant intensity is at +480 cm^{-1}, and we assign this to $16a_0^2$. Thus, ν'_{16a} in AMT is 240 cm^{-1}.

d. ν_{16b}. Since the reduced masses of DMT and AMT are similar, the excited state wave number of the nontotally symmetric mode ν_{16b} in AMT should be similar to the value of 268 cm^{-1} observed in DMT. The only transition in this area is at +267 cm^{-1}. We therefore assign this as $16b_0^2$, yielding a value of 134 cm^{-1} for ν'_{16b} in AMT. The values of ν'_{16b} in the various tetrazine derivatives should have the relationship mentioned above for ν'_{6a}. This relationship is indeed observed, as ν'_{16b}(tetrazine) = 806 cm^{-1}, ν'_{16b}(AT) = 429 cm^{-1}, and ν'_{16b}(DMT) = 268 cm^{-1}.

e. ν_2. As for the mode ν'_{16b}, the wave number of ν_2 should be similar in AMT and DMT. In DMT, ν'_2 is 1284 cm^{-1}. The only unassigned feature in this region is at +1285 cm^{-1}, which we assign to 2_0^1.

f. ν_{8a}. The mode ν_{8a} has a node passing through the ring carbon atoms. Thus, for the same reasons described for mode ν_{16a}, the wave numbers of ν_{8a} in AMT should be very similar to the wave numbers of 1485, 1470, and 1476 cm^{-1} seen for this mode in tetrazine, AT, and DMT. The only unassigned feature in this area is at +1484 cm^{-1}; we assign this as $8a_0^1$.

g. ν_I. There are two small peaks at +60 and +63 cm^{-1}, which are identified by pressure studies as hot bands. These peaks are always of equal intensity regardless of expansion conditions, and we tentatively identify them as the inversion doublet of the inversion hot band I_1^1. SVL emission spectra obtained exciting these transitions give ambiguous results (*vide infra*), hence this assignment is tentative.

2. Dispersed fluorescence spectra and ground state assignments

Figure 7 shows the dispersed emission spectrum obtained exciting the origin transition of AMT. A listing of the

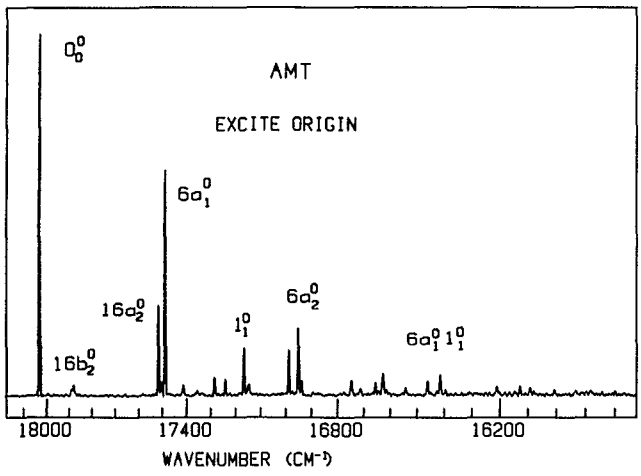

FIG. 7. The SVL dispersed emission spectrum of the AMT origin level, obtained at a resolution of 30 cm^{-1}. < 5% of the intensity of the resonance transition is due to scattered laser light.

relative frequencies, intensities, and partial assignments are given in Table II of PAPS.[22] The spectrum is dominated by a progression in ν_{6a} having a wave number of $\nu''_{6a} = 540$ cm^{-1}. The large feature at 860 cm^{-1} is the 1_1^0 transition.

SVL spectra for vibrationally excited levels can aid in determining the ground state wave numbers of the two nontotally symmetric modes ν_{16a} and ν_{16b}. SVL spectra obtained subsequent to excitation of the $16b^2$ level reveal the largest off-resonant peak to be at -150 cm^{-1}. We assign this as $16b_2^2$, yielding a value of ν''_{16b} as 75 cm^{-1}. This is similar to that of DMT ($\nu''_{16b} = 84$ cm^{-1}), and smaller than the values found in tetrazine and AT (254 and 124 cm^{-1}, respectively), reflecting changes in the reduced mass of the normal modes. Dispersing the fluorescence of the $16a^2$ level reveals a very large off-resonance peak at -512 cm^{-1}, which clearly is $16a_2^2$. This value of $\nu''_{16a} = 256$ cm^{-1} is significantly smaller than those in tetrazine (335 cm^{-1}) and DMT (349 cm^{-1}), and similar to that of AT (275 cm^{-1}). As ν''_{16a} has a node through the carbon atoms, ν''_{16a} would be expected to be similar in all of these tetrazine derivatives, and the lower value of ν''_{16a} in amino-substituted tetrazine derivatives is puzzling.

Finally, we consider the inversion mode ν_I. SVL spectra obtained exciting the two doublet components of the I_1^1 transition fail to show an anti-Stokes I_0^1 transition to the blue of the resonance excitation frequency. Hence it is not possible to extract the wave number of ν_I in the ground and excited states. The absence of the I_0^1 transition may be due to poor Franck–Condon factors for a $\Delta\nu = 1$ transition in the inversion mode, or may reflect a very small wave number for ν''_I, which causes the spacing between I_0^1 and I_1^1 to be less than our experimental resolution of 30 cm^{-1}.

3. AMT–Ar cluster spectroscopy

a. Concentration studies. As progressively more argon is added to the expansion mixture, features begin to appear to the red of the AMT monomer origin. These features clearly are attributable to AMT–argon clusters. Concentrations studies can be used to assign the cluster species responsible for each transition. The feature at 17 999 cm^{-1} grows linearly in intensity with argon concentration relative to the monomer origin, and hence is assigned as the origin transition of the AMT–Ar complex. The transition at 17 966 cm^{-1} increases approximately quadratically with increasing argon concentration; this feature is thus the AMT–Ar_2 origin transition. The two partially overlapping features on the low-wave-number edge of the AMT–Ar_2 origin increase faster than quadratically with increasing argon concentration, and are consequently due to origin transitions of AMT–Ar_n, $n > 2$. These may be the origin transitions of AMT–Ar_3 and AMT–Ar_4, respectively.

b. Cluster band shifts. From the band shift of an argon complex transition relative to the corresponding monomer transition, it is often possible to gain insight into the identity and structure of the cluster. These band shifts of the AMT–argon clusters for various vibronic transitions are summarized in Table I. The origin transition of AMT–Ar is shifted 28 cm^{-1} to the red of the monomer origin. This band shift is very similar in both magnitude and direction to the corresponding shifts in tetrazine–Ar,[28] AT–Ar,[29] and DMT–Ar.[16,26] Thus, it seems very likely that the structure of this complex is similar to the known geometries of tetrazine–Ar and AT–Ar, where the argon atom is centered ~ 3.4 Å above the aromatic ring.[28,29] The AMT–Ar_2 origin transition is red-shifted 61 cm^{-1} from the monomer origin. Within the precision of our measurements, this shift appears to be somewhat larger than twice the shift of the AMT–Ar origin transition. This violation of the band-shift rule may suggest that the two argon atoms do not occupy identical binding sites or, as is far more likely, that many-body effects cause a breakdown of the band-shift rule. The geometry of AMT–Ar_2 is almost certainly very similar to those of tetrazine–Ar_2 and AT–Ar_2, where the argon atom lies centered above and below the aromatic ring at a distance of ~ 3.4 Å.

TABLE I. Band shifts of argon cluster species relative to the corresponding AMT monomer transition.

	Number of argons in complex			
Level	1	2	3	4
0_0^0	28[a]	61	65	68
$16b_0^2$	21	54	...[b]	...
$16a_0^2$	27	63	...	...
$6a_0^1$	26	63	66	68
1_0^1	25	63	...	...
$6a_0^2$	28	58	...	...
$6a_0^1 1_0^1$	28	61	...	...
$6a_0^3$	28	58	...	...

[a] The accuracy of our measurements is estimated to be ± 1 cm^{-1}.
[b] ... indicates the corresponding transition is too weak or in too congested a spectral region to be observable.

Argon cluster transitions are also observed to the red of all higher AMT vibrational transitions. The band shifts of the argon complexes at all vibrational levels are identical within the accuracy of our experiment, with the exception of the $16b_0^2$ transition, whose cluster band shifts are somewhat smaller than those of other transitions (see Table I). This observation has implications regarding the electronic potential surface along the ν_{16b} coordinate.[30]

c. AMT–Ar origin emission. The dispersed emission spectrum obtained by exciting the zero-point origin level of AMT–Ar is virtually identical to the SVL spectra of the AMT monomer origin, with a uniform band shift of -28 cm^{-1}. No features from the uncomplexed AMT monomer are seen, which is not unexpected, since the absence of excess vibrational energy in the zero-point level prohibits vibrational predissociation of the complex. Two exceedingly weak van der Waals vibrations at -32 and -71 cm^{-1} are observed near the limit of our experimental sensitivity. These are due to the intermolecular van der Waals stretching and bending modes.

C. AMT–Ar cluster dynamics

We have obtained emission spectra of eight vibrational levels of the AMT–Ar complex. Owing to vibronic spectral congestion caused by overlapping transitions between AMT–Ar_2 and higher argon cluster oligimers, it was not possible to selectively excite AMT–Ar_2 vibrational levels and thus probe the photodissociation dynamics of di-argon complexes.

The emission spectrum obtained following excitation of $\overline{16b_0^2}$ at 274 cm^{-1} excess vibrational energy (267 cm^{-1} in the monomer) is exhibited in Fig. 8(a). The spectrum shows no features which can be attributed to fluorescence from the initially populated vibrational level. Hence, relaxation processes compete very efficiently with resonant fluorescence. All vibrational features have a full-width at half-maximum of about twice our 18 cm^{-1} experimental resolution and cannot be assigned in terms of known vibrational frequencies of the AMT monomer or argon complex.

The dispersed emission spectrum obtained exciting the $\overline{16a_0^2}$ transition at $+480$ cm^{-1} and the $\overline{6a_0^1}$ transition at $+531$ cm^{-1} can be seen in Fig. 8. Due to spectral congestion in this region, some features corresponding to the $6a_0^1$ transitions of higher argon oligimers were simultaneously excited along with $\overline{16a_0^2}$. However, this spectral contamination is estimated to be $<10\%$. No resonance emission from the $\overline{16a^2}$ or $\overline{6a^1}$ levels of the complex can be seen. Instead, the features in these spectra are identical in both position and intensity with those seen in the SVL spectrum of the AMT monomer zero-point level, indicating dissociation of the complex. A very small amount of relaxed fluorescence from a vibrationally excited level of the complex may be present at 18 000 cm^{-1} in the $\overline{6a^1}$ spectrum, but this feature is at the limit of our experimental sensitivity. Thus vibrational predissociation competes very efficiently with resonant fluorescence, and the dissociation rate thus must be fast compared to the 155 and 117 ns lifetimes[13] of the $16a^2$ and $6a^1$ levels,

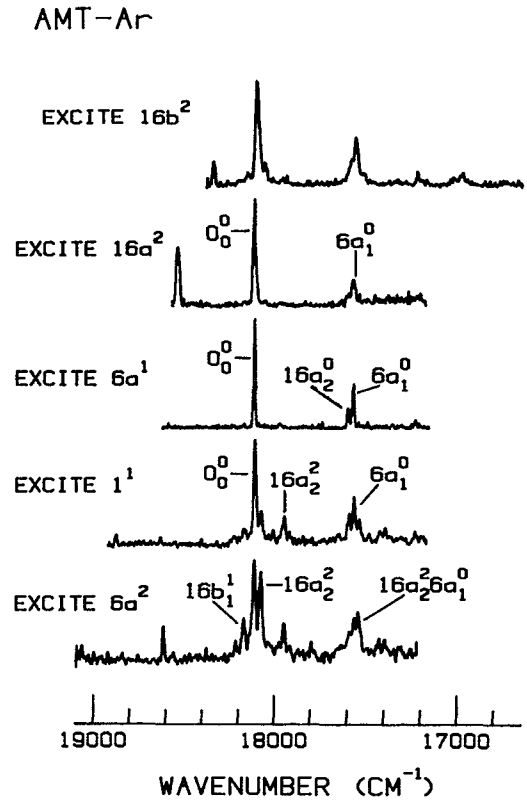

FIG. 8. (a) The dispersed emission spectrum obtained exciting the $\overline{16b_0^2}$ transition of AMT–Ar at 274 cm^{-1} excess vibrational energy, taken at a resolution of 20 cm^{-1}. All of the resonance intensity is due to scattered laser light. (b) The dispersed emission spectrum obtained exciting the $\overline{16a_0^2}$ transition of AMT–Ar at 480 cm^{-1} excess vibrational energy, taken at a resolution of 25 cm^{-1}. (c) The dispersed emission spectrum obtained exciting the $\overline{6a_0^1}$ transition of AMT–Ar at 531 cm^{-1} excess vibrational energy, taken at a resolution of 10 cm^{-1}. All of the resonance intensity in both spectra is due to scattered laser light. (d) The dispersed emission spectrum obtained exciting the $\overline{1_0^1}$ transition of AMT–Ar at 850 cm^{-1} excess vibrational energy, taken at a resolution of 13 cm^{-1}. (e) The dispersed emission spectrum of the $\overline{6a^2}$ level of AMT–Ar at 1060 cm^{-1} excess vibrational energy, taken at a resolution of 20 cm^{-1}. In all five of these traces, the transitions labeled are those of the AT photofragment.

respectively. Since dissociation is observed upon $\overline{16a^2}$ excitation (480 cm^{-1}), the binding energy of the AMT–Ar van der Waals complex must be <480 cm^{-1}.

Figure 8 also shows the emission spectrum resulting from $\overline{1_0^1}$ excitation at $+850$ cm^{-1} excess energy. Once again, cluster fragmentation occurs during the 120 ns lifetime of the 1^1 level. However, a substantial fraction of the monomer photofragments are vibrationally excited, with emission seen from the $16a^2$, $16b^2$, $16b^1$, and 0^0 levels of the AMT fragment. From the observation of $16a^2$ emission (480 cm^{-1}) following $\overline{1_0^1}$ excitation, an upper limit of 370 cm^{-1} can be set for the van der Waals binding energy. A listing of the intensities, wave numbers, and assignments of each transition is tabulated in Table II.

The $\overline{6a_0^2}$ dispersed emission spectrum at $+1062$ cm^{-1} is shown in Fig. 8(e). The spectrum is congested, making a

TABLE II. Transition in the dispersed emission spectrum obtained by exciting the AMT–Ar $\overline{1_0^1}$ transition.

ν (cm^{-1})	$\Delta\nu$ (cm^{-1})[a]	Intensity[b]	Assignment	Species
18 849	0	13	Scattered light	···
18 579	− 270	13		
18 144	− 705	18	$16b_2^2$	AMT
18 083	− 766	19	$16b_1^1$	AMT
18 026	− 824	100	0_0^0	AMT
17 989	− 859	31	$16a_2^2$	AMT
17 921	− 928	15		
17 861	− 988	31		
17 568	− 1281	14	$16b_1^1 16a_2^2$	AMT
17 508	− 1340	38	$16a_2^0$	AMT
17 484	− 1365	50	$6a_1^0$	AMT
17 458	− 1390	30	$16a_2^2\ 6a_1^0$	AMT
17 325	− 1524	19		

[a]Relative to the AMT–Ar $\overline{1_0^1}$ transition at 18 849 cm^{-1}. The accuracy of the transition frequencies is estimated to be ± 3 cm^{-1}.
[b]Intensity given relative to the highest intensity transition, which is normalized to 100. The intensity at the excitation wavelength is due to scattered laser light.

complete assignment difficult. Nonetheless, emission can be identified from the $6a^1$, $16a^2$, $16b^2$, $16b^1$, and 0^0 levels of the AMT photofragment. A tabulation of the wave numbers, intensity, and assignment of the spectral features is given in Table III.

The $\overline{6a^1 1^1}$ emission spectrum at + 1378 cm^{-1} is very broad and congested, with no resonance fluorescence observed. Evidently the $\overline{6a^1 1^1}$ level has sufficient energy that subsequent to dissociation, the AMT photofragment is vibrationally very hot, with many vibrational modes populated. Additionally, these populated modes may be of sufficiently high energy that they themselves undergo intramolecular vibrational relaxation (IVR). Consequently, the emission spectrum is broad and only partially structured, precluding a complete assignment of the modes populated by the dissociation process.

TABLE III. Transition in the dispersed emission spectrum obtained by exciting the AMT–Ar $\overline{6a_0^2}$ transition.

ν(cm^{-1})	$\Delta\nu$(cm^{-1})[a]	Intensity[b]	Assignment	Species
19 061	0	29	Scattered light	···
18 556	− 504	42	$6a_0^1$	AMT
18 133	− 928	15	$16b_2^2$	AMT
18 089	− 972	49	$16b_1^1$	AMT
18 023	− 1039	100	0_0^0	AMT
17 987	− 1074	96	$16a_2^2$	AMT
17 858	− 1203	52		
17 556	− 1505	16	$16b_1^1 6a_1^0$	AMT
17 510	− 1551	50	$16a_2^0$ or $6a_1^1 16a_2^0$	AMT
17 486	− 1575	51	$6a_1^0$	AMT
17 459	− 1602	61	$16a_2^2 6a_1^0$	AMT

[a]Relative to the AMT–Ar $\overline{6a_0^2}$ transition at 19 061 cm^{-1}. The accuracy of the transition frequencies is estimated to be ± 4 cm^{-1}.
[b]Intensity given relative to the highest intensity transition, which is normalized to 100. The intensity at the excitation wavelength is due to scattered laser light.

The dispersed emission spectrum obtained via $\overline{6a_0^3}$ excitation at 1588 cm^{-1} excess energy consists of completely broad, nearly featureless transitions devoid of any sharp structure. Thus, the initially prepared $\overline{6a^3}$ level undergoes rapid photodissociation, populating many vibrational levels of the monomer photoproduct, either directly or through IVR of the vibrationally excited AMT fragment.

IV. DISCUSSION

A. Binding energies

1. AT complexes

As discussed above, excitation of the $\overline{16b^2}$ level of AT–Ar_2 at + 462 cm^{-1} results in cluster dissociation to produce primarily the vibrationless AT photofragment. Since 462 cm^{-1} is sufficient energy to break both van der Waals bonds, then the average bond energy must be < 231 cm^{-1}. As both argon atoms bind to equivalent sites, they have the same binding energies. This upper limit of 231 cm^{-1} is considerably less than the *lower* limits for tetrazine[1] (277 cm^{-1}), 3-amino-6-methyl-*s*-tetrazine (274 cm^{-1}, *vide infra*), and dimethyltetrazine[16] (269 cm^{-1}). From the observed band shift, the ground state binding energy must be < 204 cm^{-1}.

2. AMT complexes

To determine the AMT–Ar binding energy, it is necessary to determine if $\overline{16b^2}$ excitation results in any dissociation. Excitation of $\overline{16b^2}$ gives emission from broadened vibrationally relaxed levels of either the AMT fragment or of the AMT–Ar complex. If $\overline{16b^2}$ is dissociative, the resultant AMT fragment must be vibrationally and rotationally excited, as the features in the top trace in Fig. 8 cannot be assigned as instrumentally narrow emission from the zero-point level of AMT. Vibrational levels of higher energy, such as $\overline{16a^2}$ and $\overline{6a^1}$ dissociate to the AMT zero-point level, and are of sufficiently low rotational temperatures to give transitions whose width is instrumentally limited. In every other state which undergoes dissociation, most if not all of the photofragments are left in the zero-point level. It is highly improbable that $\overline{16b^2}$ would dissociate to some unassigned level of AMT without forming any zero-point fragments. Hence, the broadened lines from relaxed vibrational states are probably not due to dissociation, but rather result from emission from mixed states of the complex. We can thus conclude that at 274 cm^{-1} excess energy, either dissociation is very slow compared to the 184 ns lifetime of $\overline{16b^2}$, or, as is far more likely, that 274 cm^{-1} is not sufficient energy to rupture the van der Waals bond. This fact, coupled with our previously

mentioned observation of $16a^2$ emission (480 cm^{-1}) following $\overline{1_0^1}$ excitation (850 cm^{-1}), enable us to bracket the excited state van der Waals binding energy as 274 $cm^{-1} < D_0' < 373$ cm^{-1}. From the observed -28 cm^{-1} band shift, the ground state binding energy can be set as 246 $cm^{-1} < D_0'' < 345$ cm^{-1}.

This reasoning also leads to the conclusion that IVR is much faster in AMT than in AT. In vibrational levels of AT–Ar ranging up to $+1212$ cm^{-1} vibrational energy, a significant amount of resonance fluorescence is observed. Conversely, in the lowest level of AMT–Ar, studied ($\overline{16b^2}$ at $+274$ cm^{-1}), IVR is already so rapid that no resonance fluorescence is visible. This is consistent with the assertion of Moss *et al.* that methyl substituents act as strong accelerating groups for IVR.[31] They hold that this acceleration effect is due not only to an increase in the vibrational density of states, but also to a mechanical coupling of the methyl rotor to the ortho-hydrogens, causing a mixing between the torsional vibrational mode and out-of-plane ring deformation modes. Of course, the AMT molecule does not have ortho-hydrogen; nonetheless, the nitrogen lone pairs may still effect sufficient steric interactions to account for the observed acceleration of the IVR rate.

B. AT–Ar dynamics

1. Relative yields

Using the intensities and assignments of the transitions observed in the dispersed emission spectra, it is possible to obtain the relative yield of dissociation product to resonance fluorescence. These raw intensities need to be corrected by two factors. First, the intensity of a transition must be weighed by its reciprocal Franck–Condon factor to take account of the fact that transitions from an excited state vibrational level can occur to many ground state vibrational levels. Second, the intensities are weighed by the inverse of the excited state fluorescence quantum yield, since peaks originating from vibrational levels having large fluorescence quantum yields will tend to be more intense than those with weaker quantum yields.

The relative yields for the AT–Ar levels calculated in this manner are shown in Table IV. The Franck–Condon factors were obtained from our SVL emission spectra of vibrationally excited levels of the AT monomer, and the quantum yields obtained from Ref. 13. The emission spectrum of the $\overline{16b^2}$ level shows no fluorescence from the initially excited level. Thus, using our knowledge of where these transitions would occur and our known experimental sensitivity, we can only determine an upper limit of the $\overline{16b^2}$ relative yield. The yields were somewhat difficult to determine for the $\overline{1^1}$ and $\overline{6a^2}$ levels, as a few of the intense peaks seen in the emission spectra were not assignable in terms of known AT vibrational modes. Thus, the Franck–Condon factors and fluorescence quantum yields of these transitions are unknown. We therefore made reasonable guesses for these quantities, enabling us to complete the analysis of these levels. However, the uncertainties in the yields and dissociation rates of $\overline{1^1}$ and $\overline{6a^2}$ are greater than in those levels in which a complete assignment of the emission spectrum was possible.

2. Dissociation rates

Since resonance fluorescence and vibrational predissociation are parallel first-order kinetic processes, the known AT fluorescence lifetimes[13] can be used to extract dissociation rates. The vibrational predissociation rates determined in this manner are shown in Table V. Since no resonance fluorescence was observed in the $\overline{16b^2}$ emission spectrum, we can only set a lower limit on its dissociation rate. These rates exhibit a strong mode selectivity, as they vary by over two orders of magnitude depending upon the initially excited mode. Interestingly, the lowest energy level, $\overline{16b^2}$ at $+446$ cm^{-1}, dissociates with the fastest rate ($> 4 \times 10^8$ s^{-1}). Stepping up in vibrational energy through $\overline{16a^2}$ ($+505$ cm^{-1}) to $\overline{6a^1}$ ($+606$ cm^{-1}), the dissociation rate *decreases* by over two orders of magnitude. If there were a dependence of the rate on energy, the dissociation rate should uniformly rise with increasing vibrational energy. Therefore it is clear that the rate depends primarily on the nature of the mode that is excited and not just on the total energy. Even at the highest level excited ($\overline{6a^2}$ at $+1212$ cm^{-1}), the dissociation rate remains slower than that of $\overline{16b^2}$, and resonance fluorescence is still seen in the emission spectrum, despite this level having many times the energy needed to break the van der Waals bond.

In the $\overline{6a^1}$ emission spectrum, the transitions resulting from the vibrationless AT photofragment are broadened due to rotational excitation. Since the rotational constants of AT are known,[12] we can use this information along with the known instrumental resolution to determine the approximate effective rotational temperature. We find that if we assume a Boltzmann distribution, then a temperature of 60 ± 10 K reproduces the spectral features well. This is much higher than the 2 K temperature with which the complexes are initially formed.[29]

C. AT–Ar_2 dynamics

1. Relative yields

The relative yields for the various vibrational levels of AT–Ar_2 are tabulated in Table VI. All of the features in the emission spectra of the $\overline{\overline{16b^2}}$, $\overline{\overline{16a^2}}$, and $\overline{\overline{6a^1}}$ levels have been assigned, as have most of the transitions in the $\overline{\overline{6a^2}}$ emission spectrum, giving us a high degree of confidence in relative yields determined for these levels. Determining the relative yields for the $\overline{\overline{1^1}}$ level is more problematic. The $\overline{\overline{1^1}}$ emission spectrum shows a series of features whose full-width at half-maximum is broadened to about twice our experimental resolution of 9.8 cm^{-1}. These features correspond in intensity and relative position to those of the AT–Ar vibrationless level, but are all uniformly shifted 18 cm^{-1} to the blue. These observations can be accounted for if the initially excited $\overline{\overline{1^1}}$ level fragments one van der Waals

TABLE IV. Relative yields for several vibronic levels of S_1 AT–Ar.

Measured fluorescence transition	Observed relative fluorescence intensity	Franck–Condon factors[a]	Fluorescence quantum yield (ϕ_n)[b]	Relative yield	Process
$\overline{16b_0^2}$ excitation:					
$\overline{16b_2^2}$	<1	0.21	0.16	<0.02	SVL fluorescence
$\overline{16b_0^2 - 356}$	<1	0.19			
0_0^0	100	0.38	0.18	>0.98	Vibrational predissociation
$16b_2^0$	4	0.02			
$16a_2^0$	7	0.03			
$6a_1^0$	52	0.25			
-670	8	0.05			
1_1^0	11	0.06			
-1160	3	0.01			
$\overline{16a_0^2}$ excitation:					
$\overline{16a_2^2}$	17	0.45	0.12	0.14	SVL fluorescence
0_0^0	100	0.38	0.18	0.86	Vibrational predissociation
$16b_2^0$	5	0.02			
$16a_2^0$	6	0.03			
$6a_1^0$	43	0.25			
-744	6	0.01			
1_1^0	13	0.06			
$\overline{6a_0^1}$ excitation:					
$\overline{6a_0^1}$	100	0.67	0.10	0.77	SVL fluorescence
$\overline{6a_0^1 16b_2^0}$	5	0.03			
$\overline{6a_1^1}$	35	0.23			
$\overline{6a_0^1 - 740}$	4	0.02			
$\overline{6a_0^1 1_1^0}$	14	0.08			
$\overline{6a_0^1 - 1057}$	6	0.02			
$\overline{6a_2^1}$	38	0.09			
$\overline{6a_2^1 - 670}$	6	0.02			
0_0^0	53	0.38	0.18	0.23	Vibrational predissociation
$6a_1^0$	27	0.25			
1_1^0	6	0.06			
$\overline{1_0^1}$ excitation:					
$\overline{1_0^1}$	24	0.27	0.10	0.17	SVL fluorescence
$\overline{1_0^1 6a_1^0}$	8	0.09			
$\overline{1_1^1}$	9	0.09			
$\overline{1_1^1 6a_1^0}$	5	0.06			
$16a_2^2$	47	0.45	0.12	0.16	Vibrational predissociation
$16a_0^2 6a_1^0$	6	0.05			
$16a_2^2 6a_1^0$	27	0.15			
$16b_1^1$	100	0.21[c]	0.17[c]	0.36	
$16b_1^1 16a_2^0$	50	0.11[c]			
0_0^0	51	0.38	0.18	0.14	
$6a_1^0$	38	0.25			
1_1^0	11	0.06			
X_π^π	82	0.45[d]	0.16[d]	0.17	
$X_\pi^\pi 6a_1^0$	24	0.25[d]			
$\overline{6a_0^2}$ excitation:					
$\overline{6a_0^2}$	45	0.60	0.07	0.15	SVL fluorescence
$\overline{6a_0^2 16b_2^0}$	3	0.04			
$\overline{6a_0^2 - 670}$	9	0.01			
$\overline{6a_0^2 - 744}$	2	0.02			
$\overline{6a_0^2 1_1^0}$	7	0.05			

TABLE IV. (*Continued.*)

Measured fluorescence transition	Observed relative fluorescence intensity	Franck–Condon factors[a]	Fluorescence quantum yield (ϕ_{fl})[b]	Relative yield	Process
$6a_0^1$	100	0.67			
$6a_0^1 16b_2^0$	6	0.03	0.10	0.19	
$6a_0^1 1_1^0$	22	0.08			
381_0^1	89	0.55			
$381_0^1 16b_2^0$	47	0.21	0.15	0.15	
0_0^0	74	0.38			Vibrational predissociation
$6a_1^0$	35	0.25	0.18	0.12	
-670	17	0.05			
All other features[e]	456	0.85[e]	0.16[e]	0.39	

[a] Taken from unpublished SVL emission spectra.
[b] Taken from Ref. 13.
[c] The Franck–Condon factors for $16b^1$ were crudely estimated using Franck–Condon factors for the $16b^2$ and 0^0 levels along with the known $\Delta v =$ even selection rules for nontotally symmetric modes. The quantum yield was estimated as in (d). These quantities must be estimated since $16b^1$ cannot be reached optically from the ground vibronic level.
[d] The vibrations labeled X_n'' and $X_n'' 6a_0^1$ cannot be assigned with known AT vibrational frequencies. We believe these to be sequence bands of an unknown vibration. Since all major features in the AT excitation spectrum have been assigned, this unknown vibrational mode must have strong $\Delta v = 0$ selection rules. We thus set the Franck–Condon factors of X_n'' and $X_n'' 6a_0^1$ equal to those of 0_0^0 and $6a_1^0$, respectively. The fluorescence quantum yields of AT monotonically decrease with increasing energy. Assuming dissociation, the level X'' must be at least several hundred cm^{-1} lower in energy than 1^1. Vibrational levels in this region have quantum yields ranging from 0.12 to 0.18; we have chosen 0.16.
[e] The intensities, Franck–Condon factors, and fluorescence quantum yields for the remaining unassigned transitions were estimated by searching for sets of peaks separated by a $6a$ spacing and using the arguments given in (d). The spectral congestion and overlapping transitions make the uncertainties of these values much greater than those described in (b).

TABLE V. Vibrational predissociation rates for several vibrational levels of AT–Ar, AT–Ar_2, and AT–Ar_3.

Level	Complex	$\Delta\nu(cm^{-1})$[a]	τ_{fl} (ns)[b]	Model[c]	Relative yields		Rates($\times 10^7$ s^{-1})[d]	
					V.P.	SVL fluor.	k_{vp}^1	k_{vp}^2
0^0	AT–Ar	0	154	···	0.00	1.00	0.0	···
$16b^2$	AT–Ar	446	143	···	>0.98	<0.02	>35	···
$16a^2$	AT–Ar	505	103	···	0.86	0.14	6	···
$6a^1$	AT–Ar	606	90	···	0.23	0.77	0.3	···
1^1	AT–Ar	798	85	···	0.83	0.17	6	···
$6a^2$	AT–Ar	1212	62	···	0.85[e]	0.15[e]	9[e]	···
0^0	AT–Ar_2	0	154	···	0.00	1.00	0.0	···
$16b^2$	AT–Ar_2	446	143	P	>0.98	<0.02	>7.4	>27
$16b^2$	AT–Ar_2	446	143	S	>0.98	<0.02	>34	>2.4
$16a^2$	AT–Ar_2	505	103	···	>0.95	<0.05	>19	···
$6a^1$	AT–Ar_2	606	90	···	0.955	0.045	24	···
1^1	AT–Ar_2	798	85	···	>0.96	<0.04	>25	···
$6a^2$	AT–Ar_2	1212	62	P	0.92	0.08	0.4	18
$6a^2$	AT–Ar_2	1212	62	S	0.92	0.08	18	48
0^0	AT–Ar_3	0	154	···	0.00	1.00	0	···
$6a^1$	AT–Ar_3	606	90	···	>0.994	<0.006	>170	···
$6a^2$	AT–Ar_3	1212	62	···	>0.987	<0.012	>130	···

[a] Relative to the origin transition of the particular complex of interest.
[b] Obtained from Ref. 13.
[c] For levels of in which only one dissociation product is observed, the data is analyzed as for AT–Ar. For levels with two dissociation products, P and S indicate analysis using the parallel and serial models, respectively.
[d] k_{vp}^1 and k_{vp}^2 are as described in the text for the parallel and serial kinetic models.
[e] For the $6a^2$ level, the many levels populated following dissociation preclude a complete assignment of the emission spectrum, as discussed in the text. Nonetheless we can obtain estimates of the relative yields. The uncertainty in these levels is larger than for the other levels.

TABLE VI. Relative yields for several vibronic levels of S_1 AT–Ar_2.

Measured fluorescence transition	Observed relative fluorescence intensity	Franck–Condon factors[a]	Fluorescence quantum yield (Φ_n)[a]	Relative yield	Process
$\overline{16b^2}$ excitation:					
$\overline{16b_2^2}$	<1	0.21	0.16	<0.02	SVL fluorescence
$\overline{16b_0^2 - 356}$	<1	0.19			
$\overline{0_0^0}$	26	0.38	0.18	0.21	Vibrational predissociation
$\overline{16b_2^0}$	1	0.02			
$\overline{16a_2^0}$	2	0.03			
$\overline{6a_1^0}$	12	0.25			
$\overline{-670}$	2	0.05			
$\overline{1_1^0}$	2	0.06			
$\overline{6a_2^0}$	3	0.05			
0_0^0	100	0.38	0.18	0.77	
$16b_2^0$	4	0.02			
$16a_2^0$	6	0.03			
$6a_1^0$	50	0.25			
-670	10	0.05			
-744	4	0.01			
1_1^0	11	0.06			
$6a_2^0$	14	0.05			
$6a_1^0 - 670$	4	0.03			
$\overline{16a^2}$ excitation:					
$\overline{16a_2^2}$	<3	0.45	0.12	<0.05	SVL fluorescence
$\overline{0_0^0}$	100	0.38	0.18	>0.95	Vibrational predissociation
$\overline{16b_2^0}$	3	0.02			
$\overline{16a_2^0}$	6	0.03			
$\overline{6a_1^0}$	43	0.25			
$\overline{-670}$	4	0.05			
$\overline{1_1^0}$	10	0.06			
$\overline{6a^1}$ excitation:					
$\overline{6a_0^1}$	4	0.67	0.10	0.045	SVL fluorescence
$\overline{6a_0^1 - 553}$	1	0.02			
$\overline{6a_1^1}$	1	0.23			
$\overline{6a_0^1 1_1^0}$	1	0.08			
$\overline{0_0^0}$	100	0.38	0.18	0.955	Vibrational predissociation
$\overline{16b_2^0}$	2	0.02			
$\overline{16a_2^0}$	6	0.03			
$\overline{6a_1^0}$	49	0.25			
$\overline{-670}$	11	0.05			
$\overline{-741}$	3	0.01			
$\overline{1_1^0}$	12	0.06			
$\overline{-1057}$	1	0.01			
$\overline{16a_2^0 6a_1^0}$	2	0.02			
$\overline{1^1}$ excitation:					
$\overline{1_0^1 6a_1^0}$	<1	0.08	0.10	<0.04	SVL fluorescence
$\overline{1_0^1 - 670}$	<2	0.09			
$\overline{1_1^1}$	<2	0.09			
$\overline{X_n^n 0_0^0}$	100	0.38	0.16	>0.96	Vibrational predissociation
$\overline{X_n^n 16b_2^0}$	2	0.02			
$\overline{X_n^n 16a_2^0}$	8	0.03			
$\overline{X_n^n 6a_1^0}$	56	0.25			
$\overline{X_n^n - 670}$	21	0.05			
$\overline{X_n^n 1_1^0}$	12	0.06			

TABLE VI. (*Continued.*)

Measured fluorescence transition	Observed relative fluorescence intensity	Franck–Condon factors[a]	Fluorescence quantum yield (Φ_{fl})[a]	Relative yield	Process
$\overline{\overline{1^1}}$ *excitation*:					
$\overline{X_n^n 16b_1^1}$	4	?	0.16	?	
$\overline{X_n^n 16b_3^1}$	5	?			
$\overline{\overline{6a^2}}$ excitation:					
$\overline{\overline{6a_0^2}}$	9	0.60	0.07	0.08	SVL fluorescence
$\overline{\overline{6a_1^2}}$	5	0.23			
$\overline{\overline{6a_0^2 1_1^0}}$	1	0.04			
$\overline{\overline{6a_2^2}}$	3	0.06			
$\overline{\overline{6a_1^2 1_1^0}}$	2	0.02			
$\overline{6a_0^1}$	4	0.47	0.10	0.02	Vibrational predissociation
$\overline{6a_1^1}$	6	0.33			
$6\,\overline{a_0^1 1_1^0}$	2	0.08			
0_0^0	82	0.38	0.18	0.22	
$6a_1^0$	45	0.25			
$16b_1^1$	100	0.55[b]	0.17[b]	0.39	
$16b_3^1$	78	0.25[b]			
$16a_2^2$	92	0.45	0.12	0.30	
$16a_2^2 6a_1^0$	46	0.30			

[a] The Franck–Condon factors and fluorescence quantum yields for the assigned modes were taken from unpublished SVL emission spectra and Ref. 13, respectively. The Franck–Condon factors and fluorescence quantum yields for combination bands involving X_n^n were estimated as given in (d) of Table IV.

[b] The Franck–Condon factors for the $16b^1$ level were crudely estimated using the Franck–Condon factors of the $16b^2$ and 0^0 levels, along with the known $\Delta v =$ even selection rules for nontotally symmetric modes. The fluorescence quantum yield for $16b^1$ was estimated as given in (d) of Table IV. These quantities cannot be determined directly since this level can not be reached optically from the ground vibronic level.

bond, with enough energy going into translational energy to drop the AT–Ar fragment to a low-lying vibrational level. The vibrational energy in this level then flows into the van der Waals mode. If enough energy goes into translational energy of the fragments, there will not be sufficient vibrational energy to rupture the remaining van der Waals bond, and emission occurs from the relaxed levels, leading to broadened emission centered near the AT–Ar origin. Even though there are many unresolved levels under each peak in Fig. 4(a), it is still possible to determine the dissociation rate. Since the van der Waals modes have strong $\Delta v = 0$ selection rules, the emission from these levels mirrors that of the AT–Ar vibrationless level, and we can use the zero-point level Franck–Condon factors for these transitions. This information, combined with an estimate of the fluorescence quantum yield for the relaxed levels, enables a determination of the relative yield for the $\overline{\overline{1^1}}$ level of AT–Ar_2. The uncertainty in this value may be somewhat larger than those of other levels.

These relative yields show a strong dependence on the initially excited modes. Excitation of $\overline{\overline{16b^2}}$ yields dissociation product of ~20% AT–Ar and ~80% AT. Excitation of the $\overline{\overline{16a^2}}$ level at $+505\ \mathrm{cm}^{-1}$ yields exclusively the AT–Ar photoproduct. Surprisingly, the highest energy level which we are able to excite, the $\overline{\overline{6a^2}}$ level at $+1212\ \mathrm{cm}^{-1}$, gives more emission from the undissociated complex than any of the levels with lower energies, including $\overline{\overline{6a^1}}$.

2. Dissociation rates: Serial vs parallel

In the dissociation dynamics of AT–Ar_2, an additional complexity is introduced, as two dissociation products, AT and AT–Ar, are possible. The dissociation of AT–Ar_2 can be envisioned as occurring in parallel,

$$\begin{array}{ccccc} \mathrm{AT}^* & \xleftarrow{k_{up}^2} & (\mathrm{AT\text{–}Ar_2})^* & \xrightarrow{k_{up}^1} & (\mathrm{AT\text{–}Ar})^* \\ \downarrow k_{fl}^2 & & \downarrow k_{fl}^{res} & & \downarrow k_{fl}^1 \\ \mathrm{AT} & & \mathrm{AT\text{–}Ar_2} & & \mathrm{AT\text{–}Ar} \end{array} \qquad (1)$$

or as a serial process,

$$\begin{array}{ccccc} (\mathrm{AT\text{–}Ar_2})^* & \xrightarrow{k_{up}^1} & (\mathrm{AT\text{–}Ar})^* & \xrightarrow{k_{up}^2} & \mathrm{AT}^* \\ \downarrow k_{fl}^{res} & & \downarrow k_{fl}^1 & & \downarrow k_{fl}^2 \\ \mathrm{AT\text{–}Ar_2} & & \mathrm{AT\text{–}Ar} & & \mathrm{AT} \end{array} \qquad (2)$$

The correct kinetic model cannot be determined from the steady-state data presented here. For those levels in which both AT and AT–Ar photoproducts are seen, we have analyzed the data both ways. By integrating the appropriate rate equations, the predicted relative yields for the two models can be obtained.

Table V lists the relative yields and dissociation rates for the five levels of AT–Ar_2. The $\overline{\overline{16a^2}}$, $\overline{\overline{6a^1}}$, and $\overline{\overline{1^1}}$ levels dissociate to yield only a single photoproduct, and the data analysis proceeds as for AT–Ar. The $\overline{\overline{16b^2}}$ and $\overline{\overline{6a^1}}$ levels yield both photoproducts, enabling k^1_{vp} and k^2_{vp} to be determined. We have analyzed these levels using both the parallel and serial models.

D. AT–Ar_3 dynamics

1. Assignment of emission spectrum

The emission spectra of the $6a^1$ and $6a^2$ levels of AT–Ar_3 show transitions which cannot be assigned in terms of known vibrational modes of AT. The $6a^2$ emission spectrum is identical to that obtained exciting the $\overline{\overline{1^1}}$ level of AT–Ar_2. If our assignment for the $\overline{\overline{1^1}}$ level is correct, then excitation of the $6a^2$ level of AT–Ar_3 results in the fragmentation of two argon atoms from the cluster, with enough energy going into translational kinetic energy to leave the AT–Ar photoproduct in a low lying vibrational level. This vibrational energy flows into the van der Waals levels, where it does not have sufficient energy to rupture the remaining AT–Ar bond. Consequently, we see relaxed, broadened emission from the AT–Ar fragment which is vibrationally populated in the van der Waals modes.

The emission spectrum of the $6a^1$ level of AT–Ar_3 is very similar to that of $\overline{\overline{1^1}}$ and the $6a^2$ level of AT–Ar_3, except there is a uniform shift of all the peaks by 27 cm^{-1} to the red. A red shift of 27 cm^{-1} corresponds to the shift of a transition upon complexation of an additional argon atom. Thus, it appears that upon excitation of the AT–Ar_3 $6a^1$ level, one argon atom is cleaved off, carrying a significant amount of translational energy. The resulting AT–Ar_2 product does not have sufficient energy to fragment further, and the excess vibrational energy relaxes into the van der Waals modes, giving broad, relaxed emission.

2. Relative yields and dissociation rates

The relative yields for the $6a^1$ and $6a^2$ levels of AT–Ar_3 are listed in Table VII. The features in these emission spectra are assigned as $\Delta v = 0$ van der Waals sequence bands in combination with transitions seen in the AT vibrationless level emission spectrum. We have thus used the Franck–Condon factors from the corresponding zero-point transitions. This information, along with an estimate for the fluorescence quantum yield, enables the relative yield to be determined.

For AT–Ar_3 complexes, three photoproducts are possible: AT–Ar_2, AT–Ar, and AT. In both of the levels studied here, only a single photoproduct is seen, thus enabling us to analyze the data in a manner similar to that used for the AT–Ar complexes. The rates are given in Table V.

E. AMT–Ar dynamics

1. Relative yields

The relative yields of levels of AMT–Ar with sharp emission spectra are given in Table VIII. Emission following excitation of the $\overline{6a^1 1^1}$ and $\overline{6a^3}$ levels is broad and nearly structureless, most likely a result of vibrational predissociation producing states of sufficiently high vibrational energy that the vibrationally hot AMT fragment undergoes IVR prior to fluorescence. This structureless emission permits only a crude estimate of the relative yield. Qualitatively, however, we can still conclude that dissociation competes very effectively with resonance fluorescence for the $\overline{6a^1 1^1}$ and $\overline{6a^3}$ levels.

In all of the levels studied, we fail to see resonance fluorescence from the initially populated vibrational mode. From our knowledge of the location and Franck–Condon factors for these transitions, we can set upper limits on the relative yield for resonance fluorescence. These also are given in Table VIII, along with the transitions whose absences were used to set these limits.

2. Dissociation rates

Since we fail to observe resonance fluorescence in all of the cluster dispersed emission spectra, it is possible only to set a lower limit on the relative yield of dissociation to resonance fluorescence. Consequently, we can only determine lower limits for vibrational predissociation rates. These are given in Table IX. These limits are all on the order of 10^8 s^{-1} or faster, with the stronger transitions having the larger lower limits, owing to increased signal to noise ratios for their emission spectra.

F. Comparison to other systems

Our data for the AT complexes can best be interpreted in terms of the large body of work which has been done on similar systems. The closest systems to which our present data can be compared are complexes between argon and various tetrazine derivatives. The first system of this type studied was tetrazine–Ar. Extensive work performed on this system revealed very little mode selectivity.[1–5] Five excited vibrational levels were studied, ranging from $+524$ to $+1406$ cm^{-1}. The dissociation rates from these levels varied by about a factor of 2, all being $\sim 1\text{–}2\times 10^8$ s^{-1}. Thus, the extreme mode selectivity seen in AT–Ar, where the dissociation rate changes by over two orders of magnitude for closely lying vibrational levels, is not an intrinsic property of the tetrazine chromophore, but is only turned on by substitution of an amino group. However, the AMT–Ar data presented here points out that all amino-substituted tetrazines do not exhibit the dramatic mode selective behavior seen in

TABLE VII. Relative yields for several vibronic levels of S_1 AT–Ar_3.

Measured fluorescence transition[a]	Observed relative fluorescence intensity	Franck–Condon factors[b]	Fluorescence quantum yield (ϕ_n)[b]	Relative yield	Process
$\overline{\overline{6a^1}}$ excitation:					
$\overline{\overline{6a_0^1}}$	>1	0.67	0.10	<0.007	SVL fluorescence
$\overline{\overline{6a_0^1 1_1^0}}$	>1	0.08			
$\overline{X_n^n 0_0^0}$	100	0.38	0.18	>0.993	Vibrational predissociation
$\overline{X_n^n 16b_2^0}$	3	0.02			
$\overline{X_n^n 16a_2^0}$	5	0.03			
$\overline{X_n^n 6a_1^0}$	54	0.25			
$\overline{X_n^n - 670}$	7	0.05			
$\overline{X_n^n - 742}$	3	0.01			
$\overline{X_n^n 1_1^0}$	11	0.06			
$\overline{\overline{6a^2}}$ excitation:					
$\overline{\overline{6a_1^2}}$	<1	0.23	0.07	<0.01	SVL fluorescence
$\overline{\overline{6a_0^2 1_1^0}}$	<1	0.04			
$\overline{Y_n^n 0_0^0}$	29	0.38	0.10	>0.17	Vibrational predissociation
$\overline{Y_n^n 6a_1^0}$	8	0.25			
$\overline{Y_n^n 1_1^0}$	3	0.06			
$\overline{Y_n^n 6a_1^0}$	6	0.04			
$\overline{X_n^n 0_0^0}$	100	0.38	0.10	>0.82	
$\overline{X_n^n 16b_2^0}$	4	0.02			
$\overline{X_n^n 16a_2^0}$	8	0.03			
$\overline{X_n^n 6a_1^0}$	54	0.25			
$\overline{X_n^n - 670}$	12	0.05			
$\overline{X_n^n - 741}$	3	0.01			
$\overline{X_n^n 1_1^0}$	12	0.06			
$\overline{X_n^n 6a_2^0}$	13	0.04			

[a] The vibration X_n^n is defined in (d) of Table IV (Y_n^n is similarly defined).

[b] The Franck–Condon factors and fluorescence quantum yields for the assigned modes were taken from unpublished SVL emission spectra and Ref. 13, respectively. The Franck–Condon factors and fluorescence quantum yields for combination bands involving X_n^n and Y_n^n were estimated as given in (d) of Table IV.

AT–Ar. Obviously other subtle factors are influencing the dissociation dynamics.

Recently we have examined the DMT–Ar complex.[21] All vibrational levels with sufficient energy fragmented with great efficiency; no resonance fluorescence was seen. The lack of time-resolved data on the DMT monomer hindered our determination of the dissociation rates to an extent; nonetheless, we were able to set a lower limit for the dissociation rate of the $\overline{6a^1}$ level ($+525\ cm^{-1}$) of $>3\times10^9\ s^{-1}$. Other levels likely dissociate at similar rates. This behavior is different from both tetrazine–Ar and AT–Ar, and very similar to that of AMT–Ar described here.

The dissociation rate for the $6a^1$ level has been measured for four different tetrazine derivatives: tetrazine–Ar, AT–Ar, AMT–Ar, and DMT–Ar. The dissociation rate for DMT–Ar and AMT–Ar are, respectively, 3×10^9 and $\geqslant1.6\times10^9\ s^{-1}$, while those of tetrazine–Ar and AT–Ar are 2×10^8 and $2\times10^6\ s^{-1}$, respectively. Thus the two methyl-containing derivatives dissociate much faster than the tetrazine and AT clusters, and have a vibrational predissociation rate an order of magnitude larger than the value of $\approx10^8\ s^{-1}$ typically found in monocyclic ring-rare gas complexes. Nimios *et al.*[32] have proposed that vibrational predissociation of van der Waals complexes occurs in a two step process, where the initially excited level undergoes IVR into the intermolecular van der Waals modes, and the complex then undergoes Rice–Ramsberger–Kassel–Marcus (RRKM) statistical dissociation. While it is exceedingly difficult to reconcile this model with the extreme mode selectivity seen in AT–Ar_n complexes, this mechanism is able to rationalize the increase in dissociation rate upon ring methylation. We note that in tetrazine–argon, emission is seen from both relaxed states of the complex and from the tetrazine fragment, indicating that both IVR and vibrational predissociation are occurring on similar time scales.[1] However, with one possible exception (*vide infra*), all of the levels populated by IVR

TABLE VIII. Relative yields for several vibronic levels of S_1 AMT–Ar.

Measured fluorescence transition	Observed relative fluorescence intensity	Franck–Condon factors[a]	Fluorescence quantum yield (ϕ_{fl})[b]	Relative yield	Process
$\overline{16a_0^2}$ excitation:					
$\overline{16a_0^2}$	<6	0.10	0.20	<0.08	SVL fluorescence
$\overline{16a_0^2 6a_1^0}$	<3	0.15			
0_0^0	100	0.33	0.29	>0.92	Vibrational predissociation
$16b_2^0$	8	0.02			
$6a_2^0$	23	0.09			
$6a_1^0$	49	0.19			
$\overline{6a_0^1}$ excitation:					
$\overline{6a_0^1}$	<0.5	0.63	0.15	<0.005	SVL fluorescence
$\overline{6a_0^1 1_1^0}$	<1.5	0.06			
0_0^0	100	0.33	0.29	>0.995	Vibrational predissociation
$16b_2^0$	6	0.02			
$16a_2^0$	20	0.09			
$6a_1^0$	48	0.19			
1_1^0	8	0.05			
$\overline{1_0^1}$ excitation:					
$\overline{1_0^1}$	<7	0.29	0.16	<0.07	SVL fluorescence
$\overline{1_0^1 6a_1^0}$	<2	0.12			
$\overline{1_2^1}$	<4	0.04			
$16a_2^2$	42	0.31	0.20	0.11	Vibrational predissociation
$16a_2^2 6a_1^0$	27	0.15			
$16b_2^2$	15	0.25	0.24	0.25	
$16b_1^1$	26	0.25[c]	0.26[c]	0.39	
$16b_1^1 16a_2^0$	10	0.12[c]			
0_0^0	100	0.33	0.29	0.18	
$16a_2^0$	27	0.09			
$6a_1^0$	38	0.19			
$\overline{6a_0^2}$ excitation:					
$\overline{6a_0^2}$	<10	0.44	0.12	<0.03	SVL fluorescence
$\overline{6a_1^2}$	<6	0.24			
$6a_0^1$	23	0.63	0.15	0.04	Vibrational predissociation
$16a_2^2$	88	0.31	0.20	0.33	
$16a_2^2 6a_1^0$	54	0.15			
$16b_2^2$	20	0.25	0.24	0.10	
$16b_1^1$	41	0.25[c]	0.27[c]	0.19	
$16b_1^1 6a_1^0$	17	0.08[c]			
0_0^0	100	0.33	0.29	0.32	
$6a_1^0$	54	0.19			

[a] Taken from unpublished SVL emission spectra.
[b] Taken from Ref. 13.
[c] See (b) in Table VI.

have wave numbers $<262\ cm^{-1}$ below the wave number of the optically prepared state, indicating that $<262\ cm^{-1}$ of vibrational energy has flowed into the van der Waals modes. Since the van der Waals binding energy is $277 < D_0' < 381\ cm^{-1}$, none of these relaxed states of the complex have yet deposited enough energy into the van der Waals modes to dissociate. Once vibrational energy $> D_0'$ flows into the van der Waals modes, dissociation evidently occurs extremely rapidly, since relaxed levels with greater than the dissociation energy in the van der Waals modes are not observed. Thus, if IVR and vibrational predissociation are sequential, IVR must be the rate limiting step, since relaxed states hav-

TABLE IX. Vibrational predissociation rates for several vibrational levels of AMT–Ar.

Excitation	$\Delta\nu$ (cm^{-1})[a]	τ_{fl} (ns)[b]	Branching ratios V.P.	Branching ratios SVL Fluor.	k_{VP} (10^8 s^{-1})
0^0	0	219	0.00	1.00	0.0
$16b^2$	274	184	0.00	1.00	0.0
$16a^2$	480	155	>0.92	<0.08	>0.9
$6a^1$	531	117	>0.995	<0.005	>16.0
1^1	850	120	>0.93	<0.07	>1.9
$6a^2$	1060	93	>0.97	<0.03	>2.1
$6a^11^1$	1378	80	>0.95[c]	<0.05[c]	>2.4[c]
$6a^3$	1588	69	>0.95[c]	<0.05[c]	>2.8[c]

[a] Relative to the AMT–Ar origin transition at 17 999 cm^{-1}.
[b] Obtained from Ref. 13.
[c] For the $6a^11^1$ and $6a^3$ levels, the extensive IVR subsequent to dissociation precludes detailed assignments in the emission spectra, as discussed in the text. Nontheless we can obtain estimates of the relative yields. The uncertainty in these levels is larger than for other levels.

ing vibrational energy $>D_0'$ never build up in sufficient intensity to be visible. The one possible exception is $\overline{16b^1}$ emission following $\overline{6a^1}$ excitation, in which 300 cm^{-1} of vibrational energy is in the van der Waals modes. Two comments may be made of this level. First, 300 cm^{-1} still may not be greater than D_0'. Second, this feature is extremely weak, having an intensity of only 0.03% of the total integrated spectral intensity.[1] Thus, even if D_0' is <300 cm^{-1}, only a tiny amount of $\overline{16b^1}$ builds up during the dissociation process, indicating that, if the sequential mechanism is valid, then IVR remains the rate limiting step.

Methylation of tetrazine has two effects. First, the increased number of vibrational modes from the methyl group will tend to decrease the rate of RRKM dissociation. Second, the methyl group will greatly increase the rate of IVR, both by increasing the density of states and by mechanically coupling to the ortho lone pairs, thus mixing the methyl rotor modes with out-of-plane ring bending modes.[31] If the vibrational predissociation rate remains faster than the IVR rate, then IVR will remain the rate limiting step, as in tetrazine–Ar. The net effect of methylation would be to increase the overall dissociation efficiency, since a methyl group increases the rate limiting step (i.e., IVR). Progressive addition of methyl groups will eventually increase the IVR rate and decrease the RRKM dissociation step to the extent that the RRKM dissociation step becomes rate limiting. This may be occurring in the dissociation of the DMT dimer,[33] where large amounts of relaxed fluorescence indicates that build-up of a large concentration of vibrationally relaxed dimer species.

Much less work has been performed on di-argon complexes. Rettschnick *et al.*[34] looked at the $\overline{6a^1}$ level of tetrazine–Ar_2. Some dissociation was observed, but, owing to weak signal levels, they could not achieve sufficient resolution to determine if the photodissociation product was tetrazine or tetrazine–Ar. Recently we looked at the DMT–Ar_2 complex.[21] In this system, the product yield appears to be a function only of the available energy. Low-lying vibrational levels fragment only one argon. When the vibrational level is of higher energy than the binding energy of the two van der Waals bonds, complete dissociation becomes very efficient, yielding only the bare DMT fragment. The behavior seen in the AT–Ar_2 complex to our knowledge is unprecedented for single ring aromatic–rare gas complexes. The large variation of the product yields as a function of the initially excited vibrational mode make this system a paradigm of mode-selective van der Waals chemistry. This simple photochemical reaction can be efficiently driven to either one of the two possible products depending upon the vibrational mode into which the energy is deposited. Thus, placing two quanta of energy into ν_{16b} produces the AT photoproduct with an 80% yield, while two vibrational quanta in higher energy ν_{16a} mode give the less-fragmented AT–Ar product with virtually 100% efficiency.

The reasons for the extreme mode selective behavior in complexes between AT and argon is not well understood, particularly since other tetrazine derivatives (tetrazine, DMT, and AMT) which are chemically and structurally very similar to AT show no such behavior. The differences in the dynamics cannot be attributed to structural differences in the complexes, as high resolution rotationally resolved spectroscopy has shown that the binding sites for the first and second argon atoms in the AT complex are identical to those observed for the tetrazine complexes.[29] The gross features of the electronic structure and electronic transitions of all these derivatives are similar, as evidenced by their similar monomer spectroscopy. Thus, the large qualitative differences in their dissociation dynamics must reflect small differences in their electronic structure. The dissociation dynamics are evidently extremely sensitive to the detailed nature of the excited electronic state.

ACKNOWLEDGMENTS

This work was supported by the National Science Foundation under Grant No. CHE-8818321. J. C. A. gratefully acknowledges support under the National Science Founda-

tion Graduate Fellowship Program. S. J. M. acknowledges support under the Illinois Minority Graduate Fellowship Program. We are indebted to Dr. D. D. Yang for synthesis of the samples of AT and AMT.

[1] D. V. Brumbaugh, J. E. Kenney, and D. H. Levy, J. Chem. Phys. **78**, 3415 (1983).
[2] J. J. F. Ramaekers, H. K. vanDijk, J. Langelaar, and R. P. H. Rettschnick, Faraday Discuss. Chem. Soc. **75**, 183 (1983).
[3] J. J. K. Ramaekers, L. B. Krignen, H. J. Lips, J. Langelaar, and R. P. H. Rettschnick, Laser Chem. **2**, 125 (1983).
[4] M. Heppener, A. G. M. Kunst, D. Bebelaar, and R. P. H. Rettschnick, J. Chem. Phys. **83**, 5341 (1985).
[5] M. Heppener, and R. P. H. Rettschnick, in *Structure and Dynamics of Weakly Bound Molecular Complexes*, edited by A. Weber (Reidel, Dordrecht, 1987).
[6] T. A. Stephenson and S. A. Rice, J. Chem. Phys. **81**, 1083 (1984).
[7] H. Abe, Y. Ohyanagi, M. Ichijo, N. Mikami, and M. Ito, J. Chem. Phys. **89**, 3512 (1985).
[8] K. W. Butz, D. L. Catlett, Jr., G. E. Ewing, D. Krajnovich, and C. S. Parmenter, J. Phys. Chem. **90**, 3533 (1986).
[9] H.-K. O, C. S. Parmenter, and M. C. Su, Ber. Bunsenges, Phys. Chem. **92**, 253 (1988).
[10] B. A. Jacobson, S. Humphrey, and S. A. Rice, J. Chem. Phys. **89**, 5624 (1988).
[11] M. R. Nimlos, M. A. Young, E. R. Bernstein, and D. F. Kelley, J. Chem. Phys. **91**, 5268 (1989).
[12] J. C. Alfano, S. J. Martinez, D. D. Yang, and D. H. Levy, J. Mol. Spectrosc. **143**, 366 (1990).
[13] J. C. Alfano, S. J. Martinez, and D. H. Levy, J. Chem. Phys. **94**, 2475 (1991).
[14] J. C. Alfano, S. J. Martinez, and D. H. Levy, J. Chem. Phys. **91**, 7302 (1989).
[15] J. C. Alfano, S. J. Martinez, and D. H. Levy, J. Chem. Soc. Faraday Trans. **86**, 2351 (1989).
[16] D. L. Osborn, J. C. Alfano, N. vanDantzig, and D. H. Levy (unpublished).
[17] R. E. Smalley, L. Wharton, and D. H. Levy, J. Mol. Spectrosc. **66**, 375 (1977).
[18] R. E. Smalley, L. Wharton, and D. H. Levy, J. Chem. Phys. **64**, 3266 (1976).
[19] D. V. Brumbaugh, C. A. Haynam, and D. H. Levy, J. Mol. Spectrosc. **94**, 316 (1982).
[20] H. H. Takimoto, and G. C. Donault, Tetrahedron Lett. **44**, 5369 (1966).
[21] A. D. Counotte-Potman and H. C. vanderPlass, J. Heterocycl. Chem. **15**, 445 (1987).
[22] See AIP document No. PAPS JCPSA-96-2522-5 for 5 pages of supplementary material Tables I and II. Order by PAPS number and journal reference from American Institute of Physics, Physics Auxiliary Publication Service, 335 East 45th Street, New York, NY 10017. The price is $1.50 for each microfiche (60 pages) or $5.00 for photocopies of up to 30 pages. Airmail additional. Make checks payable to the American Institute of Physics.
[23] K. K. Innes, L. A. Franks, H. A. Merer, G. K. Venulapalli, T. Cassen, and J. Lowry, J. Mol. Spectrosc. **66**, 465 (1977).
[24] D. V. Brumbaugh and K. K. Innes, Chem. Phys. **59**, 413 (1981).
[25] C. A. Haynam and D. H. Levy, J. Phys. Chem. **87**, 2091 (1983).
[26] C. A. Haynam, D. V. Brumbaugh, and D. H. Levy, J. Chem. Phys. **81**, 2270 (1984).
[27] R. Tembreull, T. M. Dunn, and D. M. Lubman, Spectrochim. Acta, Part A **42**, 899 (1986).
[28] C. A. Haynam, D. V. Brumbaugh, and D. H. Levy, J. Chem. Phys. **80**, 2256 (1984).
[29] J. C. Alfano, S. J. Martinez, and D. H. Levy, J. Chem. Phys. **94**, 1673 (1991).
[30] P. Weber and S. A. Rice, J. Chem. Phys. **88**, 6120 (1989).
[31] D. B. Moss, C. S. Parmenter, and G. E. Ewing, J. Chem. Phys. **86**, 51 (1986).
[32] M. R. Nimios, M. A. Young, E. R. Bernstein, and D. F. Kelly, J. Chem. Phys. **91**, 5268 (1989).
[33] C. A. Haynam, D. V. Brumbaugh, and D. H. Levy, J. Chem. Phys. **81**, 2282 (1984).
[34] J. J. F. Ramaekers, Ph.D. thesis, University of Amsterdam, 1983.